

A Three-Dimensional Constitutive Equation And Finite Element Method Implementation for Shape Memory Polymers

Guanghui Shi¹, Qingsheng Yang^{1,2}, Xiaoqiao He^{3,4}, Kim Meow Liew³

Abstract: In order to describe the thermomechanical deformation and shape memory effect of shape memory polymers (SMPs), a three-dimensional thermo-mechanical constitutive model that considers elastic, viscoelastic strain and thermal expansion is proposed for isotropic SMPs. A three-dimensional finite element procedure is developed by implementing the proposed constitutive model into the user material subroutine (UMAT) in ABAQUS program. Numerical examples are used to compare it with existing experimental data in a one dimensional case and to demonstrate the thermomechanical behavior of SMPs with 3D deformation. It is shown that the present constitutive theory and the finite element method can effectively simulate the thermomechanical behavior and shape memory effect of SMPs under complicated deformation states.

Keywords: Shape memory polymer; constitutive model; viscoelasticity; thermo-mechanics

1 Introduction

As an intelligent macromolecule material, applications of shape memory polymers (SMPs) have evoked great interest since the 1980s. Because of their light weight, good durability, large deformation and shape recovery, SMPs are being applied in areas of energy, aerospace, biomedical systems and so on [Behl, Zotzmann, and Lendlein (2010); Leng, Lan, Liu and Du (2011); Hu, Meng, Li and Ibekwe (2012); Mather, Luo and Rousseau (2009)]. SMP materials can recover to their initial shape after deformation caused by changes in external temperature and load. Thus, the

¹ Department of Engineering Mechanics, Beijing University of Technology, Beijing 100124, PR China

² Corresponding authors E-mail: qsyang@bjut.edu.cn, Tel & Fax: 86-10-67396333 (QS Yang).

³ Department of Civil and Architectural Engineering, City University of Hong Kong, Tat Chee Avenue, Kowloon, Hong Kong

⁴ Corresponding authors. E-mail: bcxqhe@cityu.edu.hk, Tel&Fax: 852-34424760 (XQ He).

storage and release of strain [Meng and Hu (2009); Nelson (2008); Lendlein and Kelch (2002)] can be achieved. Thermally isotropic SMP is the most common of such materials. Achievement of storage and release of strain is due to the occurrence of glass transition of SMPs, as the temperature changes [Hayashi, Ishikawa and Giordano (1993); Takahashi, Hayashi and Hayashi (1998)]. The thermomechanical cycle process in the SMPs involves the following four steps: loading at high temperature, cooling under constant load, unloading at low temperature and heating under free load. The elastic, viscoelastic and thermal deformation, and shape memory effect are displayed in this process. The above mentioned high and low temperatures denote temperatures above the end and below the beginning of glass transition of SMPs. To obtain relatively high mechanical properties, several researches have worked on SMP composites reinforced by carbon nanotubes [Yang, He, Liu, Leng and Mai (2012); Liu, Gall, Dunn and McCluskey (2004); Yang, Huang, Li and Chor (2005); Sahoo, Jung, Yoo and Cho (2007); Ni, Zhang, Fu, Dai and Kimura (2007)].

The constitutive models of thermotropic SMPs generally have two types, one of which is based on traditional viscoelastic theories, used to describe thermomechanical cycle process of SMPs. For example, Tobushi, Hashimoto, Hayashi and Yamada (1997) proposed a four-element constitutive model for infinitesimal deformation which involves the slip mechanism of SMPs based on the linear viscoelastic model. This model was extended to a large deformation case by adding an energy function to the system [Tobushi, Okumura, Hayashi and Ito (2001)]. But this is only a one-dimensional constitutive model and its three-dimensional version has not been found in literature. Diani, Liu and Gall (2006) presented a three-dimensional thermo-viscoelastic constitutive model for finite strain of SMPs based on the principle of energy change. Zhou, Liu and Leng (2009) formulated a 3D thermomechanical constitutive equation of SMPs. However, applications of these constitutive equations are limited due to the lack of experimental data for material parameters. Another type of constitutive model of SMPs is the micromechanics-based method, such as the phase transition and the mixture theory. Barot and Rao (2006) derived a thermomechanical constitutive equation for crystallizable SMP material based on incompressible hyperelastic model and the mixture theory. Liu, Gall, Dunn, Greenberg and Diani (2006) proposed a 3D linear elastic constitutive model for small deformation that considers the molecular mechanism of the shape memory. Chen and Lagoudas (2008a, b) established a thermomechanical constitutive model for large 3D deformation of SMPs. By taking account of the concept of phase transformation, Qi, Nguyen, Castroa, Yakacki and Shanda (2008) developed an amorphous thermomechanical constitutive relationship for finite deformation of SMPs. Li, Wang, Xiong and Chang (2009) established a thermomechanical

constitutive equation for crystallizable materials by using the theory of polymer crystallography. Srivastava, Chester and Anand (2010) gave a constitutive equation for large deformation SMP on the basis of a thermomechanical coupling theory in 2010. A review of advances of constitutive relations of SMPs was given by Zhang and Yang (2012) very recently.

However, these constitutive equations of SMPs are so complicated and contain so many material parameters that it is difficult to apply them in practical engineering. The lack of experimental data for material parameters restricts the finite element implementation of the constitutive models. It is necessary to develop applicable constitutive equations with physical definitions and the finite element procedure for complicated deformation of SMPs. Actually, the available 3D finite element program and numerical investigations are very limited in existing literature.

In this paper, by considering the elastic, viscoelastic and thermal deformation of isotropic SMPs, we propose a three-dimensional form of a thermomechanical constitutive equation for isotropic thermal actuated SMPs, with defined physical significance. A finite element procedure based on the present constitutive model is implemented by using user material subroutine(UMAT) of ABAQUS, and some numerical examples are provided to illustrate the 3D deformation and shape memory effect of SMPs.

2 Thermomechanical constitutive model of SMPs

For thermal sensitive SMPs, the total strain can be decomposed into three parts, i.e. elastic, viscoelastic and thermal strain, that is

$$\boldsymbol{\varepsilon}_{ij} = \boldsymbol{\varepsilon}_{ij}^e + \boldsymbol{\varepsilon}_{ij}^v + \boldsymbol{\varepsilon}_{ij}^T \quad (1)$$

where $\boldsymbol{\varepsilon}_{ij}$ is strain tensor and $\boldsymbol{\varepsilon}_{ij}^e$, $\boldsymbol{\varepsilon}_{ij}^v$ and $\boldsymbol{\varepsilon}_{ij}^T$ are elastic strain, viscoelastic strain and thermal strain, respectively. For the isotropic SMP, the elastic strain is

$$\boldsymbol{\varepsilon}_{ij}^e = \frac{1+\nu}{E} \sigma_{ij} - \frac{\nu}{E} \sigma_{kk} \delta_{ij} = \frac{1+\nu}{E} \sigma_{ij} - \frac{\nu}{1-2\nu} \varepsilon_{kk} \delta_{ij} \quad (2)$$

where E is the Young's modulus and ν is Poisson's ratio of the SMPs. The thermal expansion strain is expressed by

$$\boldsymbol{\varepsilon}_{ij}^T = \alpha (T - T_0) \delta_{ij} \quad (3)$$

where T is temperature, T_0 is a reference temperature and α is coefficient of thermal expansion.

It is important to describe storage and releasing effect of strain due to time-dependent viscoelastic behavior in a thermomechanical cycle process. The viscoelastic deformation can be described by combining a Kelvin and a Maxwell model [Lockett

(1972)]. The strain rate of the viscoelastic model is related with the slipping effect caused by internal friction of SMP. For the one-dimensional case, the strain rate can be written as

$$\dot{\epsilon}^v = \frac{\sigma}{\mu} - \frac{\epsilon - \epsilon^s}{\lambda} \tag{4}$$

where $\mu(T)$ and $\lambda(T)$ are viscosity coefficient and retardation time, respectively, depending on the temperature. $\epsilon^s(t, T)$ is creep residual strain, unrecovered part of the creep strain, while $\epsilon - \epsilon^s$ is retardation strain. It is noted that as the temperature is above the glass transition region, i. e. $T > T_h = T_g + T_w$, where T_g is the glass transition temperature and T_w is temperature amplitude of the glass transition region, the creep strain can be recovered completely, which means the $\epsilon^s(t, T)$ does not appear. Within the glass transition temperature region, i.e. $T_h = T_g + T_w > T > T_l = T_g - T_w$, there is a critical value of creep strain at which part of the creep strain becomes irrecoverable while for the case below glass transition temperature, the creep residual strain is a constant. Therefore, the creep residual strain has the following form...[Bhattacharyya and Tobushi (2000)]

$$\epsilon^s(t, T) = \begin{cases} 0 & \text{as } \epsilon^c(t) < \epsilon^l(T), \dot{\epsilon}^c(t) > 0 \\ C(T)(\epsilon^c(t) - \epsilon^l(T)) & \text{as } \epsilon^c(t) \geq \epsilon^l(T), \dot{\epsilon}^c(t) > 0 \\ \epsilon^s(t_1, T) & \text{as } \dot{\epsilon}^c(t) \leq 0 \end{cases} \tag{5}$$

where ϵ^c is the creep strain. t_1 denotes the moment of $\dot{\epsilon}_c(t) = 0$ as the creep strain rate varies from positive to negative. ϵ^l is a threshold value of the creep strain. $C(T)$ is a proportion coefficient.

Considering the creep residual strain in a thermomechanical process, the one-dimensional viscoelastic strain rate can be expressed by

$$\dot{\epsilon}^v(t) = \begin{cases} \frac{\sigma(t)}{\mu(T)} - \frac{\epsilon(t)}{\lambda(T)} & \text{as } \epsilon^c(t) < \epsilon^l(T) \\ \frac{\sigma(t)}{\bar{\mu}(T, C)} - \frac{\epsilon(t) - \bar{\epsilon}^s(T, C)}{\bar{\lambda}(T, C)} & \text{as } \epsilon^c(t) \geq \epsilon^l(T), \dot{\epsilon}^c(t) > 0 \\ \frac{\sigma(t)}{\mu(T)} - \frac{\epsilon(t) - \epsilon^s(t_1, T)}{\lambda(T)} & \text{as } \dot{\epsilon}^c(t) \leq 0 \end{cases} \tag{6}$$

where the viscosity coefficient $\mu(T)$ and retardation time $\lambda(T)$ in the glass transition region is replaced by

$$\bar{\mu}(T, C) = \mu(T) \left[1 - \frac{C(T)\mu(T)}{E(T)\lambda(T)} \right]^{-1}, \quad \bar{\lambda}(T, C) = \lambda(T) [1 - C(T)]^{-1} \tag{7}$$

The creep residual strain ϵ^s in the glass transition region is modified as

$$\bar{\epsilon}^s(T, C) = -\frac{C(T)\epsilon^l(T)}{1 - C(T)} \tag{8}$$

Based on the viscoelastic correspondence principle of solid mechanics [Lockett (1972); Dunne and Petrinic (2005)], the three-dimensional form of Eq.6 can be expressed by

$$\dot{\epsilon}_{ij}^v = \begin{cases} \frac{\sigma_{ij}}{\mu} - \frac{\epsilon_{ij}}{\lambda} - \frac{1}{3} \left(\frac{E}{\mu(1-2\nu)} - \frac{1}{\lambda} \right) \delta_{ij} \epsilon_{kk}, & \text{as } \bar{\epsilon}^c(t) < \epsilon^l(T) \\ \frac{\sigma_{ij}}{\mu} - \frac{\epsilon_{ij} - \bar{\epsilon}^s(T,C) \delta_{ij}}{\lambda} - \frac{1}{3} \left(\frac{E}{\mu(1-2\nu)} - \frac{1}{\lambda} \right) \delta_{ij} \epsilon_{kk}, & \text{as } \bar{\epsilon}^c(t) \geq \epsilon^l(T), \dot{\bar{\epsilon}}^c(t) > 0 \\ \frac{\sigma_{ij}}{\mu} - \frac{\epsilon_{ij} - \epsilon^s(t_1, T) \delta_{ij}}{\lambda} - \frac{1}{3} \left(\frac{E}{\mu(1-2\nu)} - \frac{1}{\lambda} \right) \delta_{ij} \epsilon_{kk}, & \text{as } \dot{\bar{\epsilon}}^c(t) \leq 0 \end{cases} \quad (9)$$

where the creep strain in the three-dimensional case is calculated by

$$\bar{\epsilon}^c(t) = \bar{\epsilon}(t) - \frac{\bar{\sigma}(t)}{E(T)} \quad (10)$$

where $\bar{\epsilon}$ and $\bar{\sigma}$ are the Mises equivalent values of strain ϵ_{ij} and stress σ_{ij} , respectively.

By using Eqs. (1), (2), (3) and (9), we obtain three-dimensional constitutive equation of SMPs in a rate form

$$\begin{aligned} \dot{\epsilon}_{ij} + \frac{5\nu - 1}{3(1 - 2\nu)} \delta_{ij} \dot{\epsilon}_{kk} \\ = \begin{cases} \frac{(1+\nu)\dot{\sigma}_{ij}}{E} + \frac{\sigma_{ij}}{\mu} - \frac{\epsilon_{ij}}{\lambda} - \frac{1}{3} \left(\frac{E}{\mu(1-2\nu)} - \frac{1}{\lambda} \right) \delta_{ij} \epsilon_{kk} + \alpha \dot{T} \delta_{ij}, & \text{as } \bar{\epsilon}^c(t) < \epsilon^l(T) \\ \frac{(1+\nu)\dot{\sigma}_{ij}}{E} + \frac{\sigma_{ij}}{\mu} - \frac{\epsilon_{ij} - \bar{\epsilon}^s(T,C) \delta_{ij}}{\lambda} - \frac{1}{3} \left(\frac{E}{\mu(1-2\nu)} - \frac{1}{\lambda} \right) \delta_{ij} \epsilon_{kk} + \alpha \dot{T} \delta_{ij}, & \text{as } \bar{\epsilon}^c(t) \geq \epsilon^l(T), \dot{\bar{\epsilon}}^c(t) > 0 \\ \frac{(1+\nu)\dot{\sigma}_{ij}}{E} + \frac{\sigma_{ij}}{\mu} - \frac{\epsilon_{ij} - \epsilon^s(t_1, T) \delta_{ij}}{\lambda} - \frac{1}{3} \left(\frac{E}{\mu(1-2\nu)} - \frac{1}{\lambda} \right) \delta_{ij} \epsilon_{kk} + \alpha \dot{T} \delta_{ij}, & \text{as } \dot{\bar{\epsilon}}^c(t) \leq 0 \end{cases} \quad (11) \end{aligned}$$

In Eq.11, the viscosity coefficient μ , retardation time λ and coupling coefficient C are dependent on the temperature due to the glass transition of SMPs. The constitutive equations, with the temperature-dependent parameters, can reflect the thermo-mechanical behavior of different types of SMP materials. One-dimensional form of Eq.11 is coincident with results of Tobushi, Hashimoto, Hayashi and Yamada (1997).

For comparing the results, the shape memory polymer of polyurethane series is investigated in the present paper. It is assumed that the SMP maintains a set of

material parameters when the temperature is less than the lower limit of the glass transition temperature. Similarly, when the temperature is greater than the upper limit of the glass transition temperature range, the SMP material maintains another set of material constants. However, within the range of glass transition of SMPs, material parameters are strongly temperature-dependent, which can be expressed as

$$X = X_g \exp \left[k_x \left(\frac{T_g}{T} - 1 \right) \right] \tag{12}$$

where T_g is the glass transition temperature, X denotes one of the material parameters E , μ , λ , C and ϵ_l . k_x is a coefficient corresponding to parameter X . Differing from shape memory alloys [Liu, Dui and Zhu (2011); Chen, Peng, Chen, Wang and Hu (2012)], the materials data of the SMPs is very limited. Specific material parameters of polyurethane series ...[Tobushi, Hashimoto, Hayashi and Yamada (1997); Bhattacharyya and Tobushi (2000)]are listed in Tables 1 to 3.

Tables 1 and 2 provide the coefficients within the glass transition region and Table 3 gives the material parameters outside the glass transition region where T_w is amplitude of glass transition temperature. Meanwhile, the coefficient of thermal expansion α and Poisson’s ratio are the same within and beyond the glass transition region. For polyurethane system, the glass transition temperature T_g is about 328K, temperature amplitude T_w is about 15K and the glass transition region is, therefore, about 313~343K.

Table 1: Values of parameters at glass transition temperature

$E_g(\text{MPa})$	$\mu_g(\text{Gpa.s})$	$\lambda_g(s)$	C_g	$\epsilon_{l,g}(\%)$
146	14	521	0.112	0.3

Table 2: Values of coefficients k_x

k_E	k_μ	k_λ	k_C	k_{ϵ_l}
38.1	44.2	35.4	38.7	-58.2

3 Finite element implementation

A user routine UMAT of ABAQUS was written to implement the present constitutive equations. It has been verified that the multifield finite element method is

Table 3: Values of material parameters at $T \geq T_g + T_w$ and $T \leq T_g - T_w$

parameters	$T \geq T_g + T_w$	$T \leq T_g - T_w$
$E(\text{MPa})$	27.6	907
$\mu(\text{GPa} \cdot \text{s})$	2.03	116
$\lambda(\text{s})$	111	2840
C	0.0206	0.716
$\varepsilon^l(\%)$	3.83	0.0184
$\alpha(K^{-1})$	11.6e-5	
ν	0.3	

a powerful tool to deal with the multifield coupling problem, such as fluid-solid interaction [Ma, Bernard, Yang and Yang (2011)] and chemo-mechanical coupling [Yang, Liu and Meng (2009)]. The specific procedures for the finite element implementation are as follows:

- (1) Read the incremental load steps and temperature variables at the start time from ABAQUS program. Then, the subroutines are called to obtain material parameters at the current temperature.
- (2) Calculate the elastic stiffness matrix and select the corresponding stress update algorithm and then calculate the current stress and strain and determine the change direction of the creep strain rate according to Eq.10.
- (3) If the creep strain rate is negative, creep residual strain is equal to $\varepsilon^s(t_1, T)$ where t_1 is determined by $\dot{\varepsilon}^c(t) = 0$, and then the stress is updated according to the third equation in Eq.11.
- (4) If the creep strain rate is positive and creep strain is larger than the threshold value ε^l at the current temperature, the stress update is deducted according to the second equation in Eq.11.
- (5) If the creep strain rate is positive and the creep strain is less than threshold values ε^l at the current temperature, stress is updated according to the first equation in Eq.11.
- (6) Carry out iterative calculation according to the corresponding Jacobian matrix for each stress update, check convergence of the iteration and end the calculation.

Based on the above procedure, a FORTRAN subroutine was compiled and embedded into finite element software ABAQUS/STANDARD. The flowchart of the program is shown in Figure 1.

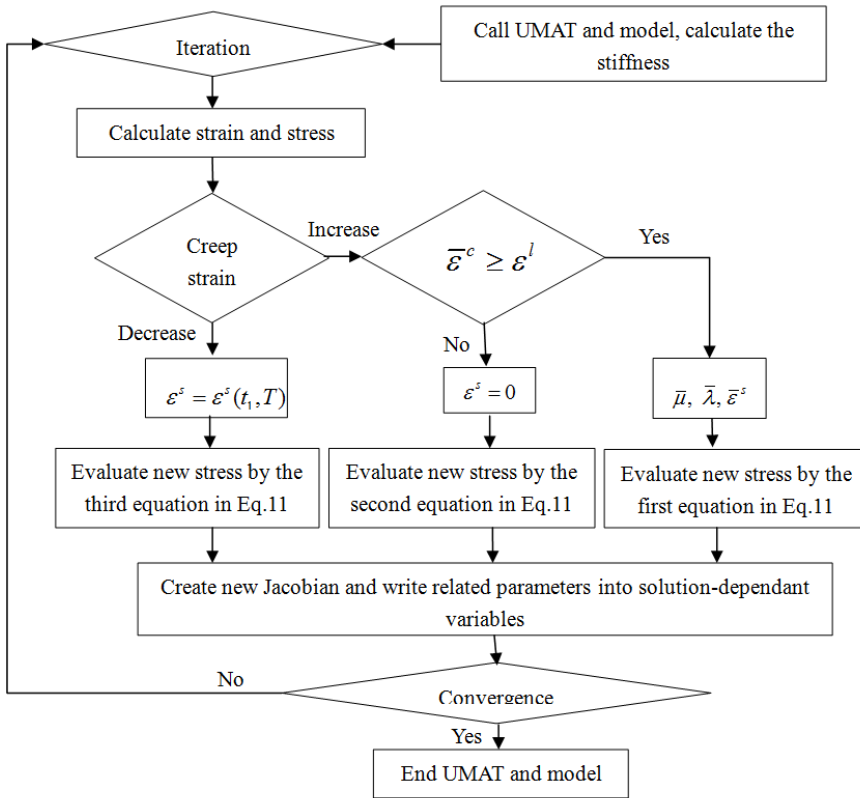


Figure 1: Flowchart of FE analysis

4 Numerical examples and result discussions

4.1 Uniaxial tensile test

For comparison with experimental data, a uniaxial tensile model is investigated first. The model size is 10*10*50mm. Boundary conditions are set as follows: one end in the length direction is fixed and a specific displacement is imposed on the other end. At Step 1 (loading), a strain rate of 1.25%/min at T=343K is applied up to 10% strain. At Step 2 (cooling), under the constant 10% strain state, temperature is reduced from 343K to 313K at the rate of 4K/min, until the cooling process is complete. At Step 3 (unloading), temperature is kept at 313K and the external load is removed, completing the unloading process at the low constant temperature. It can be seen that a part of the storage strain recovers. At Step 4 (recovery), under the free external load state, temperature rises from 313K to 343K,

completing the recovery process of the strain by heating. The curve between stress and strain is shown in Figure 2. At the high temperature state, the relatively large strain leads to obvious relaxation. This simple one-dimensional example exhibits good agreement of the present numerical results with experimental data [Tobushi, Hashimoto, Hayashi and Yamada (1997)] .

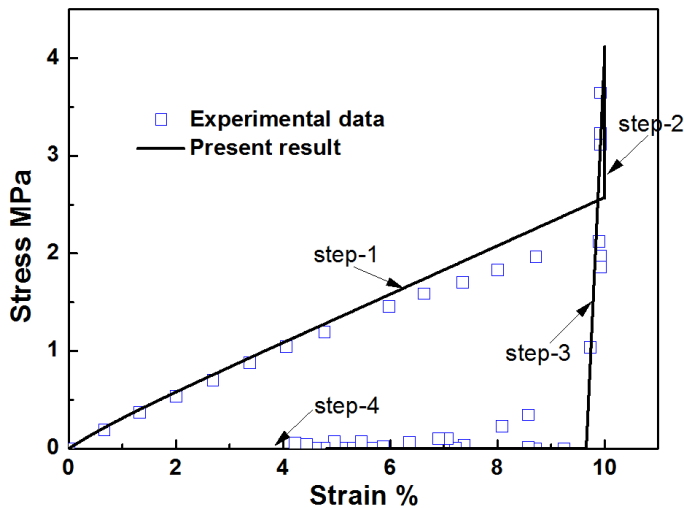


Figure 2: Comparison of numerical and experimental results

4.2 Bending of cantilever SMP beam

A deformation and shape memory effect of a cantilever SMP beam is demonstrated in this numerical example. A specific displacement is applied at the end of the beam with size 5mm*5mm*50mm. The loading rate is set as 0.5mm/min, cooling rate is 6K/min and unloading rate is 0.5mm/min. Here the influence of heating rate on the final recovery process is addressed.

The finite element model of cantilever SMP beam is shown in Figure 3. The 8-node cubic element C3D8 is used in this model with a total of 1250 elements.

Figures 4 and 5 depict variational curves of load and displacement and load and temperature, respectively, of SMP beam, when loading rate is 0.5mm/min, cooling rate is 6K/min, unloading rate is 0.5mm/min and heating rate is 0.5K/min. It can be seen that load-displacement curves of the beam are similar to the uniaxial tensile

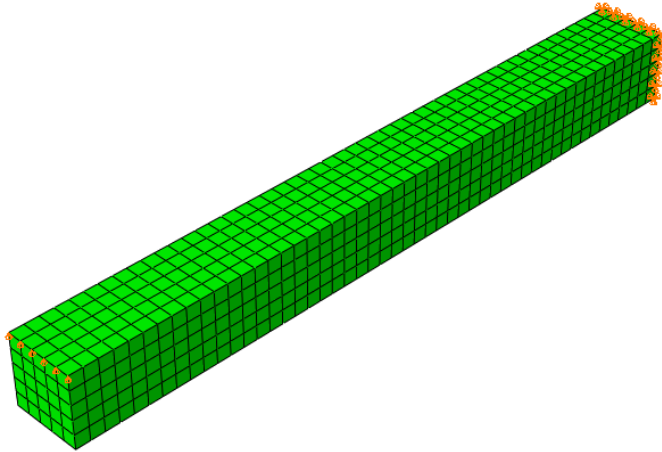


Figure 3: Finite element model of SMP beam

test. These figures show deformation and shape memory effect of SMP beam in a thermomechanical cycle process.

Figure 6 shows the relations between displacement and temperature for different temperature change rates. It can be seen that heating rate has a significant impact on the residual strain. As the heating rate decreases from 6K/min to 0.5K/min, the residual displacement decreases apparently. When heating rate is 0.5K/min, there is a very small part of the residual displacement because of assumption of the residual creep strain. Meanwhile, when the heating rate is 0.5K/min, the recovery speed of the displacement becomes small, nearly at $T=343\text{K}$. The reason is that the creep effect plays a leading role in the recovery process. The bending deformation and shape recovery of SMP beam shows that there exists a small part of residual strain in the recovery process. This example provides evidence of effectiveness of present constitutive equation and finite element procedure.

4.3 Indentation of SMP block

This example presents a numerical model for indentation of a SMP body. The model size of SMP is $20 \times 20 \times 10\text{mm}$. The indenter is simplified into a rigid hemispherical tip with radius of 1mm. Due to the symmetry of the model, we can analyze 1/4 model as shown in Figure 7. The load is applied on the rigid indenter. The contact surface between the rigid indenter and surface of SMP body is identified. A total of 8355 cubic elements are used in this example.

Figures 8 to 10 present the loading process under different working conditions. Figures 8 and 9 show variation of the indenter displacement and applied load under

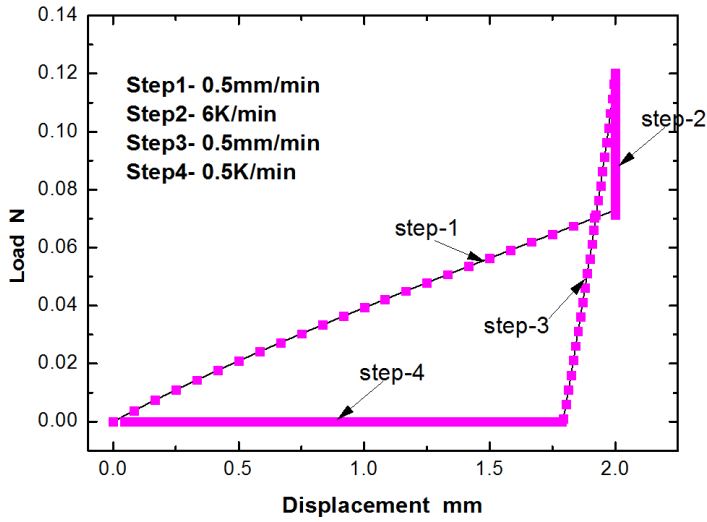


Figure 4: Relations between displacement and load of SMP beam

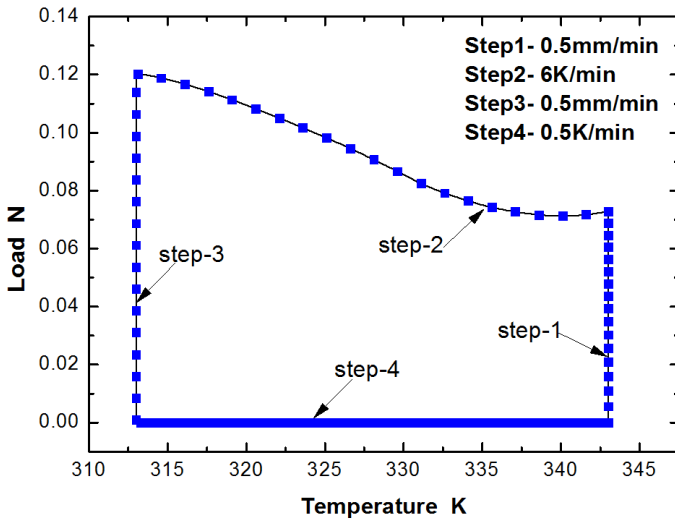


Figure 5: Relations between temperature and load in SMP beam

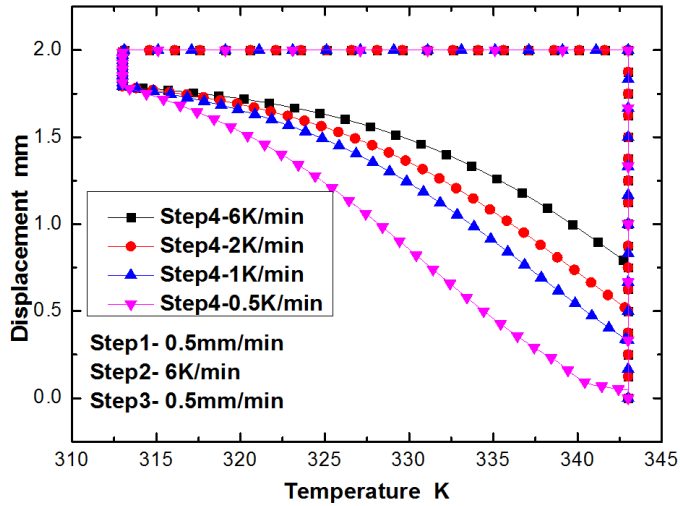


Figure 6: Relations between displacement and temperature of beam under different cooling rate

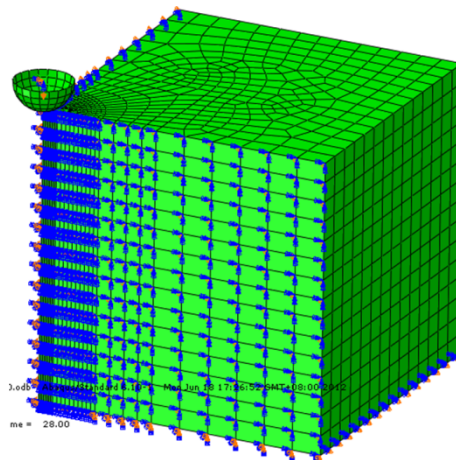


Figure 7: Finite element model of indentation of SMP body

different loading rates where the temperatures are at 313K and 343K, respectively. It can be seen from Figure 8 that loading rate has a significant impact on curves of the applied load and displacement of the indenter. The lower the loading rate is, the more obvious is the nonlinearity of the load-displacement curves. The main reason for this phenomenon can be attributed to the viscoelastic properties of the SMP material, which leads to the creep strain as loading. Similarly, as the temperature rises above the upper limit of the glass transition temperature range, material parameters remain stable. It can be seen from Figure 9 that loading strain rate has no significant effect on load-displacement curves. The reason is that SMP material properties tend to elasticity under this state. This agrees with experimental findings in existing literature [Bhattacharyya and Tobushi (2000)] .

Figure 10 demonstrates the relationship between load and displacement for the same loading rate and different temperatures in the thermomechanical cycle process. Due to the rate-dependent behavior of material properties of SMPs, they vary dramatically at the upper limit and lower limit of glass transition temperature. For the lower temperature, nonlinearity of the load-displacement curve appears for the same loading rate.

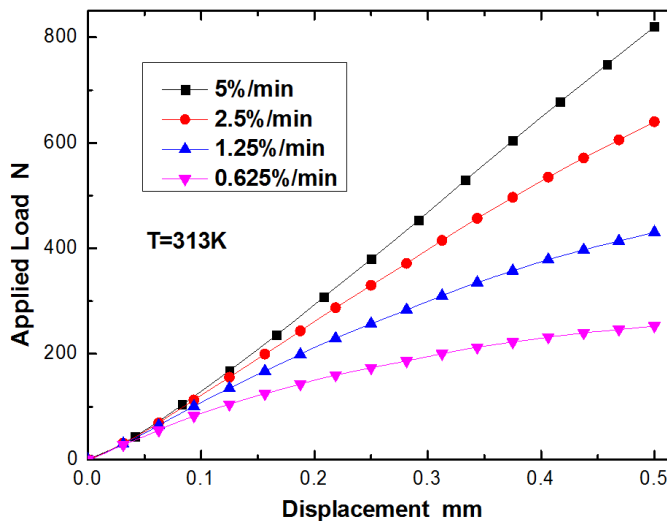


Figure 8: Relations between load and displacement at T=313K

Figure 11 shows a complete process of thermomechanical cycle where the inden-

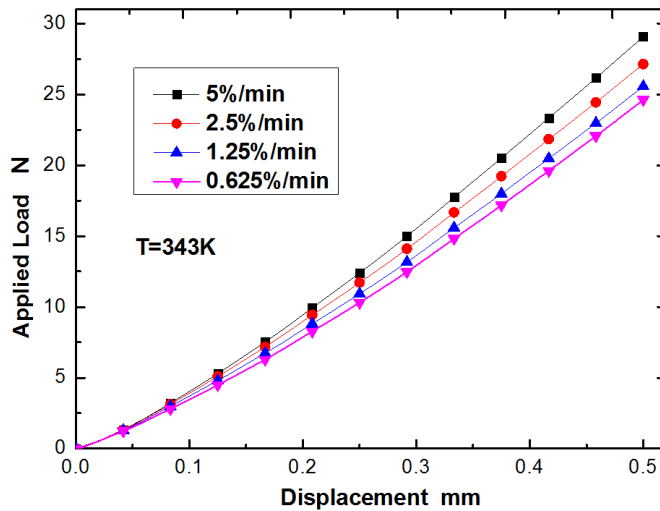


Figure 9: Relations between load and displacement at T=343K

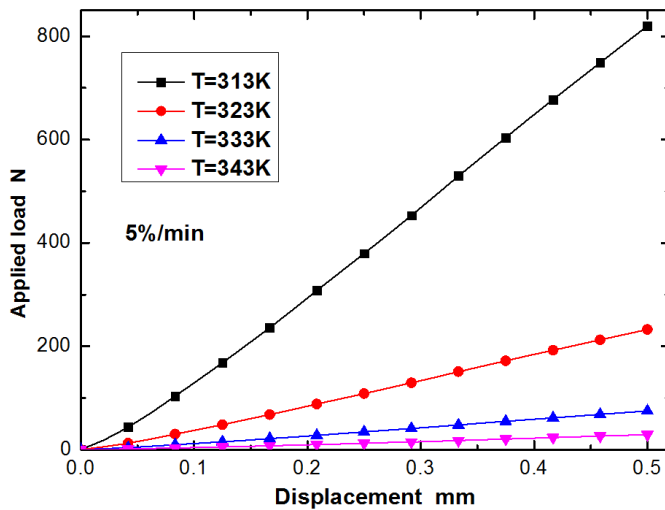


Figure 10: Relations between load and displacement at loading rate of 5%/min for different

tation morphology changes and stress clouds in the vertical direction are plotted. In the whole cycle, the loading rate is 0.5mm/min (Step 1), cooling rate is 6K/min (Step 2), unloading rate is 0.5mm/min (Step 3) and heating rate is 2K/min (Step 4). It is indicated that the final residual strain becomes very small after unloading.

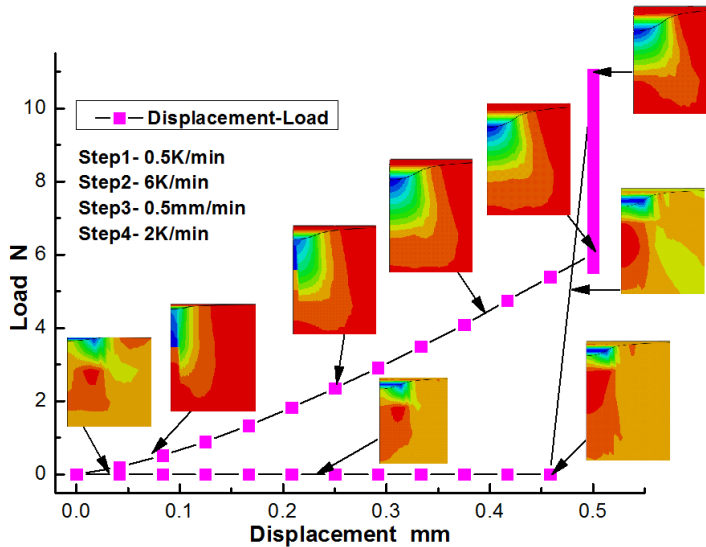


Figure 11: Variation of the indentation morphology in a whole process

Figure 12 shows the relationship between applied load and displacement under four different loading rates. The loading rate at the high temperature state can impact the peak value of the ultimate force of the indenter, but the difference is relatively small. With decrease of the loading rate, peak value of the force acting on the indenter shows a downward trend, while the whole trend of the curves remains unchanged. Furthermore, change of peak value in the loading process leads to changes of the peak value in the cooling segment. It can be seen in the case of unchanged cooling rate that increment of the force in the cooling segment remains a fixed value; the conclusions are consistent with Tobushi, Hashimoto, Hayashi and Yamada (1997) for the one-dimensional state.

Figure 13 displays the relations between load and displacement under different cooling rates. It is shown that in the cooling process, for a constant strain, the force acting on the indenter is different. Due to the thermal expansion and the increase of Young's modulus with decrease of the temperature, the change of cooling rate has an obvious influence on the peak force of the SMPs.

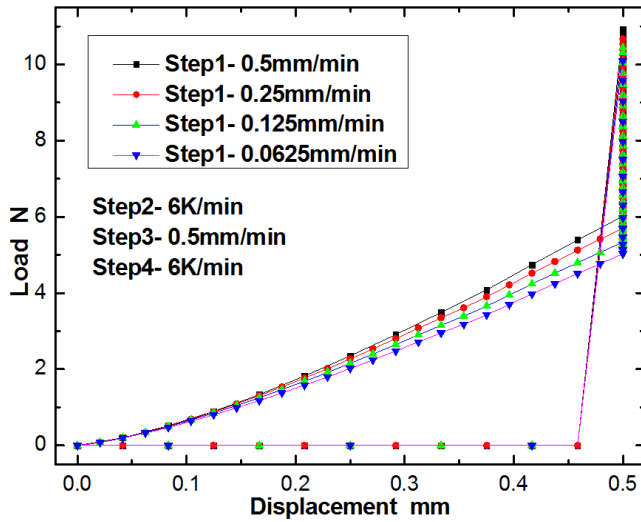


Figure 12: Relations between load and displacement under different loading rates in the loading process

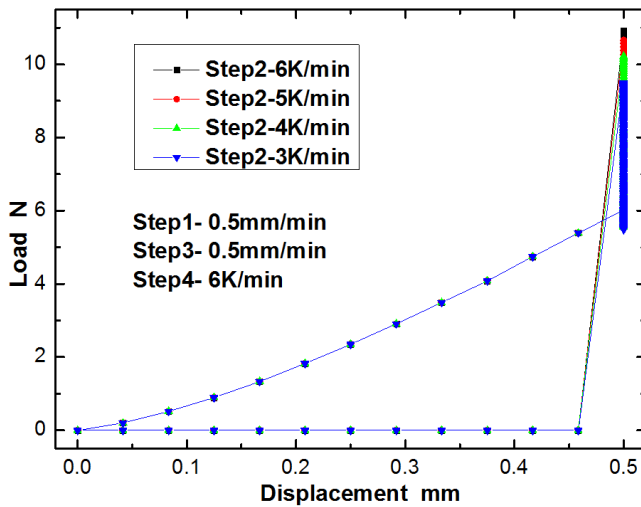


Figure 13: Relations between load and displacement for different cooling rates in the cooling process

The relations between applied load and displacement for different unloading rates in the unloading process are given in Figure 14 where the loading rate is 0.5mm/min, cooling rate is 6K/min and heating rate is 6K/min. It is found that different cooling rates have no significant effect on the unloading strain. The reason is that the unloaded deformation is the elastic strain which is in proportion with Young's modulus. We can find that the heating rate can affect the final residual strain. The recovery process under free load is controlled by the viscosity of SMPs.

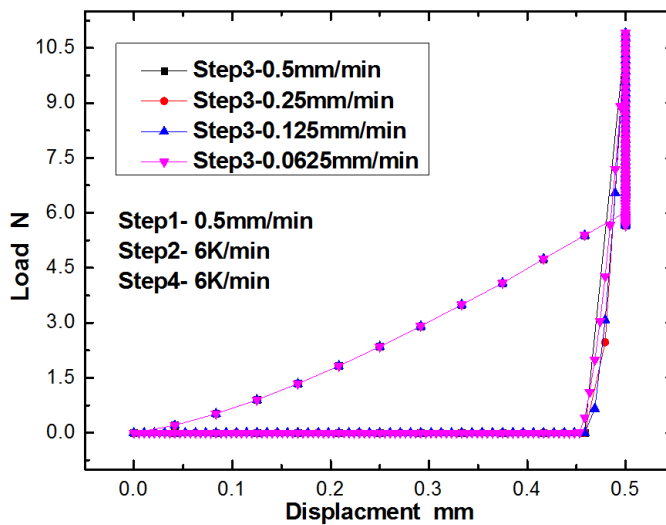


Figure 14: Relations between load and displacement under different unloading rates

5 Conclusions

In this paper, a three-dimensional thermomechanical constitutive equation of SMPs is built, considering the elastic, viscoelastic and thermal strains based on the isotropic assumption of the materials. In the framework of the user subroutines in ABAQUS, the constitutive model is implemented by coding a UMAT program. Reliability of the constitutive equations and finite element procedure are validated by several numerical examples. Behaviors of bending of a SMP beam and indentation of a SMP body are illustrated by the developed material model. The numerical results show that the present 3D thermomechanical constitutive model can be used effectively

to describe the complicated mechanical behavior of SMPs. Moreover, the thermo-mechanical behavior of SMPs is sensitive to the loading/unloading rate and cooling/heating rate. These rate-dependent behaviors are clearly shown in the present numerical examples. Therefore, it is of vital importance to have reasonable control over the rate of both loading/unloading and cooling/heating. Another application of this model and the FE procedure might be modeling of the combined elastic and SMP structures.

Acknowledgement: The financial supports from the Natural Science Foundation of China under grant #11172012 and the Research Grants Council of the Hong Kong Special Administrative Region under grant #CityU 113809 are gratefully acknowledged.

References

- Barot, G. and Rao, I. J. (2006):** Constitutive modeling of the mechanics associated with crystallizable shape memory polymers. *Z. Angew. Math. Phys.*, vol. 57, pp. 652-681.
- Bhattacharyya, A. and Tobushi, H. (2000):** Analysis of the isothermal mechanical response of a shape memory polymer rheological model. *Polym. Eng. Sci.*, vol. 40, pp. 2498-2510.
- .Behl, M.; Zotzmann, J. and Lendlein, A. (2010):** Shape-Memory Polymers and Shape-Changing Polymers. *Adv. Polym. Sci.*, vol.226, pp. 1-40.
- Chen, Y. C. and Lagoudas, D. C. (2008a):** A constitutive theory for shape memory polymers. Part I - Large deformations. *J. Mech. Phys. Solids*, vol. 56, pp. 1752-1765.
- Chen, Y. C. and Lagoudas, D. C. (2008b):** A constitutive theory for shape memory polymers. Part II - A linearized model for small deformations. *J. Mech. Phys. Solids*, vol.56, pp. 1766-1778.
- Chen, B.; Peng, X.; Chen, X.; Wang, J.; Wang, H. and Hu, N. (2012):** A Three-Dimensional Model of Shape Memory Alloys under Coupled Transformation and Plastic Deformation. *CMC: Computers, Materials & Continua*, Vol. 30, No. 2, pp. 145-176.
- Diani, J.; Liu, Y. P. and Gall, K. (2006):** Finite strain 3D thermoviscoelastic constitutive model for shape memory polymers. *Polym. Eng. Sci.*, vol. 46, pp. 486-492.
- Dunne, F. and Petrinic, N. (2005):** *Introduction to computational plasticity*. Oxford University Press, USA.

Hayashi, S.; Ishikawa, N. and Giordano, C. (1993): High moisture permeability polyurethane for textile applications. *J. Indus. Text.*, vol. 23, pp. 74-83.

Hu, J. L.; Meng, H. P.; Li, G. Q. and Ibekwe, S. I. (2012): A review of stimuli-responsive polymers for smart textile applications. *Smart Mater. Struct.*, vol. 21, pp. 053001.

Lockett, F. (1972): *Nonlinear viscoelastic solids*. Academic Press London, London.

Liu, B. F.; Dui, G. S. and Zhu, Y. P. (2011): A Constitutive Model for Porous Shape Memory Alloys Considering the Effect of Hydrostatic Stress. *CMES: Computer Modeling in Engineering & Sciences*, vol. 78, No. 4, pp. 247-276.

Liu, Y. P.; Gall, K.; Dunn, M. L.; Greenberg, A. R. and Diani, J. (2006): Thermomechanics of shape memory polymers: Uniaxial experiments and constitutive modeling. *Int. J. Plast.*, vol. 22, pp. 279-313.

Liu, Y. P.; Gall, K.; Dunn, M. L. and McCluskey, P. (2004): Thermomechanics of shape memory polymer nanocomposites. *Mech. Mater.*, vol. 36, pp. 929-940.

Lendlein, A. and Kelch, S. (2002): Shape-memory polymers. *Angew. Chem. Int. Edit.*, vol. 41, pp. 2034-2057.

Leng, J. S.; Lan, X.; Liu, Y. J. and Du, S. Y. (2011): Shape-memory polymers and their composites: Stimulus methods and applications. *Prog. Mater. Sci.*, vol. 56, pp. 1077-1135.

Li, Z. F.; Wang, Z. D.; Xiong, Z. Y. and Chang, R. N. (2009): Thermomechanical Constitutive Equations of Shape Memory Polymers. *Acta Polym. Sin.*, vol. 6, pp. 23-27.

Ma, L. H.; Bernard, F. R.; Yang, Q. S. and Yang, C. H. (2011): The Configuration Evolution and Macroscopic Elasticity of Fluid-filled Closed Cell Composites: Micromechanics and Multiscale Homogenization Modeling. *CMES: Computer Modeling in Engineering & Sciences*, Vol. 79, No. 2, pp. 131-158.

Meng, Q. H. and Hu, J. L. (2009): A review of shape memory polymer composites and blends. *Composites Part A*, vol. 40, pp. 1661-1672.

Mather, P. T.; Luo, X. F. and Rousseau, I. A. (2009): Shape Memory Polymer Research. *Annu. Rev. Mater. Res.*, vol. 39, pp. 445-471.

Nelson, A. (2008): Stimuli-responsive polymers - Engineering interactions. *Nat. Mater.*, vol. 7, pp. 523-525.

Ni, Q. Q.; Zhang, C. S.; Fu, Y. Q.; Dai, G. Z. and Kimura, T. (2007): Shape memory effect and mechanical properties of carbon nanotube/shape memory polymer nanocomposites. *Compos. Struct.*, vol. 81, pp. 176-184.

Qi, H. J.; Nguyen, T. D.; Castroa, F.; Yakacki, C. M. and Shanda, R. (2008): Finite deformation thermo-mechanical behavior of thermally induced shape memory polymers. *J. Mech. Phys. Solids*, vol. 56, pp. 1730-1751.

Srivastava, V.; Chester, S. A. and Anand, L. (2010): Thermally actuated shape-memory polymers: Experiments, theory, and numerical simulations. *J. Mech. Phys. Solids*, vol. 58, pp. 1100-1124.

Sahoo, N. G.; Jung, Y. C.; Yoo, H. J. and Cho. J. W. (2007): Influence of carbon nanotubes and polypyrrole on the thermal, mechanical and electroactive shape-memory properties of polyurethane nanocomposites. *Compos. Sci. Technol.*, vol. 67, pp. 1920-1929.

Takahashi, T.; Hayashi, N. and Hayashi, S. (1998): Structure and properties of shape-memory polyurethane block copolymers. *J. Appl. Polym. Sci.*, vol. 60, pp. 1061-1069.

Tobushi, H.; Hashimoto, T.; Hayashi, S. and Yamada, E. (1997): Thermomechanical constitutive modeling in shape memory polymer of polyurethane series. *J. Intell. Mater. Syst. Struct.*, vol. 8, pp. 711-718.

Tobushi, H.; Okumura, K.; Hayashi, S. and Ito, N. (2001): Thermomechanical constitutive model of shape memory polymer. *Mech. Mater.*, vol.33, pp. 545-554.

Yang, B.; Huang, W. M.; Li, C. and Chor, J. H. (2005): Effects of moisture on the glass transition temperature of polyurethane shape memory polymer filled with nano-carbon powder. *Eur. Polym. J.*, vol. 41, pp 1123-1128.

Yang, Q. S.; He, X. Q.; Liu, X.; Leng, F. F. and Mai, Y. W. (2012): The effective properties and local aggregation effect of CNT/SMP composites. *Composites Part B*, vol. 43, pp. 33-38.

Yang, Q. S.; Liu, B. S. and Meng, L. T. (2009): A Phenomenological Theory and Numerical Procedure for Chemo-Mechanical Coupling Behavior of Hydrogel, *CMC: Computers, Materials & Continua*, vol.353, no.1, pp.1-17.

Zhou, B.; Liu, Y. J. and Leng, J. S. (2009): Finite Element Analysis on Thermo-Mechanical Behavior of Styrene-Based Shape Memory Polymers. *Acta Polym. Sin.*, vol. 6, pp. 525-529.

Zhang, Q. and Yang, Q. S. (2012): Recent Advance on Constitutive Models of Thermal-Sensitive Shape Memory Polymers. *J. Appl. Polym. Sci.*, vol. 123, pp. 1502-1508.